International Journal of Recent Development in Engineering and Technology
Website: www.ijrdet.com (ISSN 2347 -6435 (Online)), Volume 14, Issue 12, December 2025)

Analysis of turbulent natural convection in a semi-circular enclosure filled with MWCNT/water nanofluid heated partially from the bottom

Abel Omondi Onyango[1], Johana Kibet Sigey[2], Moffat Nyaboe Chamuchi[3]

[1,2]*Department of Pure and Applied Mathematics, Jomo Kenyatta University of Agriculture and Technology, Nairobi, Kenya.*

[3]*Department of Pure and Applied Sciences, Kirinyaga University, Kerugoya, Kenya.*

***Abstract*— This research explored the analysis of turbulent natural convection in a semi-circular enclosure filled with multi-walled carbon nanotube-water nanofluid heated partially from the bottom for heating and cooling of electronic chip. The governing equations in the flow were continuity, momentum, energy and species concentration equations which were modeled in the form of partial differential equations with initial and boundary conditions. The modeled differential equations were discretized using finite difference scheme and the resulting equations solved with the help of MATLAB software to obtain the result which were presented in graphs and contours. The results showed that the heater length ratio and volume fraction have a significant impact on the distribution of heat and mass in the semi-circular enclosure. Engineering fields that need cooling systems, like electronic cabins, thermal energy storage systems and geothermal energy systems can benefit from the study's project results.**

Keywords—Turbulent, natural convection, multi-walled carbon nanotube (MWCNT), single-walled carbon nanotube (SWCNT), semi-circular enclosure.

I. INTRODUCTION

In modern electronic systems, there has been an increasing trend towards designing smaller electronic chips. This has resulted in a steady rise in heat dissipation per unit volume within an electronic enclosure. For electronic components to function correctly, their temperature must remain below the manufacturer's specified limit.

Managing the heat in electronic components is crucial for chip performance. Many traditional coolants, like air and water, have limited thermal performance because of their low heat conductivity.

Alam *et. al* [1] studied magnetohydrodynamic flow on convective heat transfer in a semi-circular cavity under lamina regime. They used the finite element method (FEM) for simulation and determined that as the Rayleigh number increases, the time it takes for the system to reach a steady-state solution decrease.

In [3], Islam and his fellow researchers conducted a study on the impact of natural convection heat transfer performance in a semi-circular cavity with a nanofluid which included the effects of Brownian motion and particle size and shape while ignoring thermophoresis and viscous dissipation. The research showed that the inclination angle of the magnetic field had the most significant impact on flow.

In 2025, Nadeem, Siddiqua and Alzabut [4] investigated the flow of hybrid nanofluid comprising single-walled carbon nanotubes (SWCNT)and multi-walled carbon nanotubes (MWCNT) within a semi-circular enclosure with a corrugated wall as an application. The aim was to study the effect of volume fraction on heat transfer applying finite element method in laminar flow. This study concluded that heat transfer is enhanced with higher solid particle volume fractions.

Nouraei *et. al.* [5], presented a study on heat transfer and entropy analysis for mixed convection with nanofluid in a semi-circular open cavity. The purpose was to find the optimal position of the heater to improve heat transfer in a circular cavity, utilizing the finite volume method. The findings indicated that most fluid exchange was caused by natural convection from density differences because the velocity of fluid motion was low in the circular components.

In 2020, Singh [6] focused on free convection with MWCNT/water nanofluid, considering the aspect ratio of MWCNT nanoparticles in a thermally undulated enclosure under laminar flow. His results concluded that the maximum aspect ratio had heat transfer performance.

Yousefzadeh *et. al.* [7] presented natural convection of multi-walled carbon nanotube-water nanofluid flow inside a semi-circular enclosure with viscous dissipation,

International Journal of Recent Development in Engineering and Technology
Website: www.ijrdet.com (ISSN 2347 -6435 (Online)), Volume 14, Issue 12, December 2025)

Brownian motion, and thermophoresis neglected. A finite volume method (FVM) was used for the simulation and the results indicate that increased Rayleigh number becomes a stronger driver for the formation of the vortex of the fluid. The objective of this paper is to analyze the effects of fluid flow parameters on turbulent fluid flow field.

The paper is organized as follows. In Section II, the mathematical problem is formulated in which the assumptions and governing equations are given in Sections III and IV respectively. The method of solution is discussed in Section V with the results and discussion given in Section VI. Conclusions and recommendations are drawn in Section VII.

II. Mathematical Formulation

The flow configuration considered turbulent natural convection in a semi-circular enclosure filled with multi-walled carbon nanotube-water nanofluid heated partially from the bottom for heating and cooling of electronic chip.

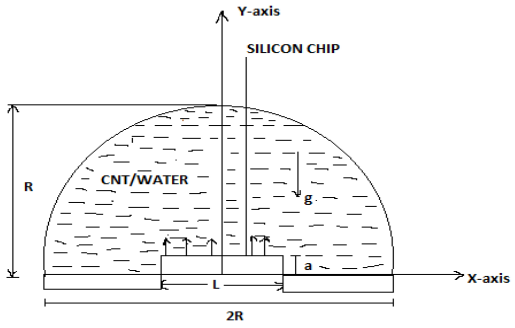

Figure 1: Heat flow configuration.

Figure 1 illustrates a schematic representation of a semi-circular cavity with a radius R=1m that's filled with a nanofluid made from multi-walled carbon nanotubes and water. In this setup, the water and MWCNT nanoparticles are in thermal equilibrium. At the center of the base wall, there's a silicon chip that generates a heat flux 'q' when it heats up. This is indicated by the vertical arrows in the y-direction emerging from the silicon chip. This chip has a length 'L' and a thickness 'a'. The other walls of the base are thermally insulated, while the curved walls are in the colder zones and are treated as adiabatic. Initially, we assume that the concentration of the nanofluid is higher, denoted as C_h, at the center of the base wall and lower, labeled as C_l, at the curved walls.

III. Assumptions

i. The flow is two-dimensional, meaning the flow variables depend only on two space coordinates.
ii. The fluid is Newtonian and incompressible, with constant density.
iii. Density changes linearly with temperature, and the deviation from a reference value is small.
iv. The induced magnetic field is negligible.
v. The flow is unsteady due to finite disturbances from the dissipative heat source energy resulting from viscous dissipation. The lamina-turbulence transition is assumed to occur at Re ≤ 3000.
vi. The ratio a/R is negligible so that the thickness 'a' of the silicon chip is not considered in the study.

IV. Governing Equations

A. Continuity equation

The conservation of mass principle tells us that in any closed system, where no external forces are acting, the mass remains constant, no matter how it deforms. We can express the continuity equation in tensor form.
The equation shows that the flow is continuous

$$\frac{\partial \overline{\rho}}{\partial t} + \frac{\partial}{x_j}(\overline{\rho u_j} + \overline{\rho^* u^*_j}) = 0$$

1) The penalty formulation technique

The technique used to eliminate the pressure term in the Navier Stokes equation. In the formulation, the continuity equation is viewed as incompressibility constrained that the velocity field must be obeyed. The approximate relationship between the pressure field and the velocity field replaces the continuity equation. Fang [2] extends a locally adaptive penalty algorithm originally introduced for the Stokes problem to the non-linear, time-dependent incompressible Navier-Stokes equations. The penalty relation takes the form according to Fang [2];

$$\frac{P}{\lambda} + \frac{\partial u_i}{\partial x_i} = 0$$

For constant property flows where the penalty parameter $\lambda = \mathrm{Re}.\mu.\omega$ and ω is arbitrary large number between 10^3 to 10^7

International Journal of Recent Development in Engineering and Technology
Website: www.ijrdet.com (ISSN 2347 -6435 (Online)), Volume 14, Issue 12, December 2025)

Re is the Reynolds number and μ is the molecular viscosity. At higher limit of the penalty parameter λ, the solution of the penalty formulation converges to that of the original Navier Stokes equation. We can therefore use penalty formulation method to eliminate the pressure term in the Navier Stokes equation. From the equation, the turbulent pressure term can be written as;

$$\overline{P} = -\mathrm{Re}.\mu.\omega \frac{\partial u_i}{\partial x_i}$$

The continuity equation is now coupled in the momentum equation to replace the pressure field and solved as velocity field in the momentum equation.

B. Momentum equation

The principle of momentum conservation is essentially a way to apply Newton's second law of motion to a group of fluid particles that are in motion. It tells us that the total of both surface and body forces acting on a system is equal to how much the momentum changes over time. When you find a balance between these forces and the rate at which momentum changes, you arrive at a general equation for momentum conservation in unsteady incompressible flow.

1) Turbulent momentum equation in the x direction

$$\frac{\partial \overset{*}{U}}{\partial t} + \overset{*}{U}\frac{\partial \overset{*}{U}}{\partial x} + \overset{*}{V}\frac{\partial \overset{*}{U}}{\partial y} = \frac{\mu_{nf}}{\rho_{nf}}(\mathrm{Re}.\omega + 1)(\frac{\partial^2 \overset{*}{U}}{\partial x^2})$$

$$+ \frac{\mu_{nf}}{\rho_{nf}}\frac{\partial^2 \overset{*}{U}}{\partial y^2} - (\nu_t)\frac{\partial}{\partial x}\left(\frac{\partial \overset{*}{U}}{\partial y} + \frac{\partial \overset{*}{V}}{\partial x}\right)$$

2) Turbulent momentum equation in the y direction

$$\frac{\partial \overset{*}{V}}{\partial t} + \overset{*}{U}\frac{\partial \overset{*}{V}}{\partial x} + \overset{*}{V}\frac{\partial \overset{*}{V}}{\partial y} = \frac{\mu_{nf}}{\rho_{nf}}(\mathrm{Re}.\omega + 1)\frac{\partial^2 \overset{*}{V}}{\partial y^2}$$

$$+ \frac{\mu_{nf}}{\rho_{nf}}\frac{\partial^2 \overset{*}{V}}{\partial x^2} - \nu_t\frac{\partial}{\partial y}\left(\frac{\partial \overset{*}{U}}{\partial y} + \frac{\partial \overset{*}{V}}{\partial x}\right)$$

$$+ \frac{(\beta_T \rho)_{nf}}{\rho_{nf}} g(\overset{*}{T} - \overset{*}{T_c}) + \frac{(\beta_c \rho)_{nf}}{\rho_{nf}} g(\overset{*}{C} - \overset{*}{C_c})$$

where ω is arbitrary large number between 10^3 to 10^7 representing the penalty parameter constant,

C. Equation of conservation of Energy

This is derived from the first law of thermodynamics which states that the rate of energy increase in a system is equal to the heat added to the system and work done on the system.

$$\left(\frac{\partial \overset{*}{T}}{\partial t} + \overset{*}{U}\frac{\partial \overset{*}{T}}{\partial x} + \overset{*}{V}\frac{\partial \overset{*}{T}}{\partial y}\right) = \alpha_{nf}\left(\frac{\partial^2 \overset{*}{T}}{\partial x^2} + \frac{\partial^2 \overset{*}{T}}{\partial y^2}\right)$$

$$+ 2\frac{\mu_{nf}}{(\rho c_p)_f}\left((\frac{\partial \overset{*}{U}}{\partial x})^2 + (\frac{\partial \overset{*}{V}}{\partial y})^2 + (\frac{\partial \overset{*}{V}}{\partial x} + \frac{\partial \overset{*}{U}}{\partial y})^2 + (\frac{\partial \overset{*}{U}}{\partial x})^2\right)$$

$$- \frac{\nu_t}{P_{r_t}}(\frac{\partial \overset{*}{T}}{\partial x} + \frac{\partial \overset{*}{T}}{\partial y}) + \frac{(\rho c_p)_p}{(\rho c_p)_f}\left(\begin{array}{l} D_B(\frac{\partial \overset{*}{T}}{\partial x}\frac{\partial \overset{*}{C}}{\partial x} + \frac{\partial \overset{*}{T}}{\partial y}\frac{\partial \overset{*}{C}}{\partial y}) \\ + \frac{D_T}{T_c}((\frac{\partial \overset{*}{T}}{\partial x})^2 + (\frac{\partial \overset{*}{T}}{\partial y})^2 \end{array}\right)$$

D. The concentration equation

It is based on the principle of mass concentration for each species in a fluid mixture. It describes the physical phenomena where particles, energy or other physical quantities are transformed inside a physical system due to convection and diffusion. For the unsteady incompressible nanofluid fluid flow, the turbulent form of the diffusion equation is

$$\frac{\partial \overset{*}{C}}{\partial t} + \overset{*}{U}\frac{\partial \overset{*}{C}}{\partial x} + \overset{*}{V}\frac{\partial \overset{*}{C}}{\partial y} = D_B(\frac{\partial^2 \overset{*}{C}}{\partial x^2} + \frac{\partial^2 \overset{*}{C}}{\partial y^2})$$

$$+ \frac{D_T}{T_c}(\frac{\partial^2 \overset{*}{T}}{\partial x^2} + \frac{\partial^2 \overset{*}{T}}{\partial y^2})$$

$$+ \frac{\nu_t}{S_{C_t}}(\frac{\partial^2 \overset{*}{C}}{\partial x^2} + \frac{\partial^2 \overset{*}{C}}{\partial y^2})$$

E. Non-dimensional form of governing equations

The following are the similarity variables chosen according to Yousefzadeh [7] with the fluid flow parameters; Reynolds number Re, thermal Grashof's number Gr_T, mass grashof's number Gr_C, Lewis number Le, Brinkman's number Br, Pecklet number Pe, Prandtl number Pr, Brownian motion parmeter number N_B, thermophoresis

International Journal of Recent Development in Engineering and Technology
Website: www.ijrdet.com (ISSN 2347 -6435 (Online)), Volume 14, Issue 12, December 2025)

parameter number N_T, volume fraction ϕ and heater length ratio parameter $\varpi = \frac{L}{R}$.

$$U = \frac{\overset{*}{U}L}{\alpha_f}, \quad V = \frac{\overset{*}{V}L}{\alpha_f}, \quad X = \frac{x}{L}, Y = \frac{y}{L}, \quad \theta = \frac{T - T_C}{T_h - T_c},$$

$$\phi = \frac{C - C_C}{C_h - C_c}, \quad \eta = \frac{\alpha_f t}{L^2} \text{ and}$$

$$q_O^{"} = \frac{k_f (T_h \_ T_C)}{L}, \quad \mathrm{Re} = \frac{\rho UL}{\mu} = \frac{UL}{\nu},$$

$$\mathrm{Pr} = \frac{\nu}{\alpha} = \frac{\mu c_p}{k}, \quad Gr_T = \frac{\beta_T g L^3 (T_h - T_C)}{\nu_f^2},$$

$$Gr_C = \frac{\beta_C g L^3 (T_h - T_C)}{\nu_f^2}, \quad Pe = \frac{UL}{\alpha_f} = \mathrm{Re} \times \mathrm{Pr},$$

$$Br = \frac{\mu U^2}{k(T_h - T_C)} = \mathrm{Pr} \times Ec,$$

$$Le = \frac{L(C_h - C_C)}{\rho c_p (T_h - T_C)} = \frac{\alpha_f}{D_B},$$

$$N_T = \frac{D_T}{T_C} \frac{(\rho c_p)_p (T_h - T_C)}{(\rho c_p)_f UL},$$

$$D_B = D_B \frac{(\rho c_p)_p (C_h - C_C)}{(\rho c_p)_f UL}, \varpi = \frac{L}{R}$$

1) Modeled x-momentum equation

$$\frac{\partial U}{\partial \eta} + U\frac{\partial U}{\partial X} + V\frac{\partial U}{\partial Y} = M_0 P_r (R_e.\omega + 1)\frac{\partial^2 U}{\partial X^2} +$$

$$M_0 P_r \frac{\partial^2 U}{\partial Y^2} + M_1 \frac{\partial^2 U}{\partial X \partial Y} + \frac{\partial^2 U}{\partial X^2}$$

Modeled y-momentum equation

$$\frac{\partial V2)}{\partial \eta} + U\frac{\partial V}{\partial X} + V\frac{\partial V}{\partial Y} = M_0 P_r (R_e.\omega$$

$$+1)\frac{\partial^2 V}{\partial Y^2} + M_0 P_r \frac{\partial^2 V}{\partial X^2} + M_1 \left(\frac{\partial^2 U}{\partial Y^2} + \frac{\partial^2 V}{\partial X \partial Y} \right) +$$

$$M_2 \theta Gr_T P_r^2 + M_3 \phi Gr_C P_r^2$$

3) Modeled concentration equation

$$\frac{\partial \phi}{\partial \eta} + U\frac{\partial \phi}{\partial X} + V\frac{\partial \phi}{\partial Y} = \frac{1}{L_e}\left(\frac{\partial^2 \phi}{\partial X^2} + \frac{\partial^2 \phi}{\partial Y^2}\right)$$

$$+ M_7\left(\frac{\partial^2 \phi}{\partial X^2} + \frac{\partial^2 \phi}{\partial Y^2}\right) + \frac{1}{L_e}\frac{N_T}{N_B}\left(\frac{\partial^2 \theta}{\partial X^2} + \frac{\partial^2 \theta}{\partial Y^2}\right)$$

Where the constants $M_0, M_1, M_2, M_3, M_4, M_5, M_6$ and M_7 are given below:

$$M_o = \frac{\nu_{nf}}{\nu_f}, \quad M_1 = -\frac{\nu_t}{\alpha_f}, \quad M_2 = \frac{(\beta_T \rho)_{nf}}{\rho_{nf}(\beta_T)_f},$$

$$M_3 = \frac{(\beta_C \rho)_{nf}}{\rho_{nf}(\beta_C)_f}$$

$$M_4 = \frac{K_{nf}}{K_f}, \quad M_5 = 2\frac{\mu_{nf}}{\mu_f}, \quad M_6 = -\frac{\nu_t}{\mathrm{Pr}_t} \text{ and}$$

$$M_7 = \frac{\rho C_p \nu_t}{k_f Sc_t}$$

F. Boundary conditions

The imposed boundary conditions according to Alarm [1] are;

1) Initial setting

$\overset{*}{U} = 0, \overset{*}{V} = 0, \overset{*}{T} = T_C, \overset{*}{C} = C_L$ and t=0.

2) Bottom surface

$\overset{*}{U} = 0, \overset{*}{V} = 0, \overset{*}{T} = T_h, \overset{*}{C} = C_h$ and t>0.

3) Circular surface

$\overset{*}{U} = \overset{*}{V} = 1, \overset{*}{T} = T_C, \overset{*}{C} = C_L$, t>0 and y=R=1

International Journal of Recent Development in Engineering and Technology
Website: www.ijrdet.com (ISSN 2347 -6435 (Online)), Volume 14, Issue 12, December 2025)

V. METHOD OF SOLUTION

The partial derivatives of U, V, C and T at each grid point are expressed using finite difference approximation. $U_{i,j}^{k}$, $V_{i,j}^{k}$, $T_{i,j}^{k}$ and $C_{i,j}^{k}$ for each i are calculated directly from the initial value condition.
Space derivatives are approximated using central difference method obtained from Taylor series approximation. The length of each interval is Δx=b units in the x-axis direction, Δy=h units in the y-axis direction, and $\Delta\eta = n$ units in the t-axis direction. This is done to help obtain an approximation to the values of U, V, C and T at the various grid points in the enclosure. For instance $U_{i,j}^{k}$ and $C_{i,j}^{k}$ denote the approximation for the horizontal velocity and the concentration values respectively at the grid point(i, j, k).

A. Discretization of momentum equations

We consider momentum equations in both vertical direction (y-axis) and horizontal directions (x-axis)

1) Discretized x-momentum equation

$$\frac{U_{i,j}^{k+1}-U_{i,j}^{k}}{n}+U_{i,j,}^{k}\frac{U_{i+1,j}^{k}-U_{i-1,j}^{k}}{2b}+V_{i,j,}^{k}\frac{U_{i,j+1}^{k}-U_{i,j-1}^{k}}{2h}=$$

$$M_0P_r(R_e.\omega+1)\frac{U_{i+1,j}^{k}-2U_{i,j}^{k}+U_{i-1,j}^{k}}{b^2}+$$

$$M_0P_r\frac{U_{i,j+1}^{k}-2U_{i,j,k}^{k}+U_{i,j-1}^{k}}{h^2}+$$

$$M_1\frac{U_{i+1,j+1}-U_{i+1,j-1}^{k}-U_{i-1,j+1}^{k}+U_{i-1,j-1}^{k}}{4bh}+\frac{U_{i+1,j}^{k}-2U_{i,j}^{k}+U_{i-1,j}^{k}}{b^2}$$

2) Discretized y-momentum equation

$$\frac{V_{i,j}^{k+1}-V_{i,j,}^{k}}{n}+U_{i,j,}^{k}\frac{V_{i+1,j}^{k}-V_{i-1,j}^{k}}{2b}+$$

$$V_{i,j,}^{k}\frac{V_{i,j+1}^{k}-V_{i,j-1}^{k}}{2h}=M_0P_r(R_e.\omega+1)\frac{V_{i,j+1}^{k}-2V_{i,j}^{k}+V_{i,j-1}^{k}}{h^2}+$$

$$M_0P_r\frac{V_{i+1,j}^{k}-2V_{i,j}^{k}+V_{i-1,j}^{k}}{b^2}+$$

$$M_1\left(\frac{U_{i,j+1}^{k}-2U_{i,j,}^{k}+U_{i,j-1}^{k}}{h^2}+\frac{V_{i+1,j+1}-V_{i+1,j-1}^{k}-V_{i-1,j+1}^{k}+V_{i-1,j-1}^{k}}{4bh}\right)$$

$$+.M_2\theta Gr_TP_r^2+M_3\phi Gr_CP_r^2$$

B. Discretized energy equation

$$\frac{\theta_{i,j}^{k+1}-\theta_{i,j}^{k}}{n}+U_{i,j,}^{k}\frac{\theta_{i+1,j}^{k}-\theta_{i-1,j}^{k}}{2b}+V_{i,j,}^{k}\frac{\theta_{i,j+1}^{k}-\theta_{i-1,j}^{k}}{2h}=M_4\left(\frac{\theta_{i+1,j}^{k}-2\theta_{i,j}^{k}+\theta_{i-1,j}^{k}}{b^2}+\frac{\theta_{i,j+1}^{k}-\right.$$

$$+M_5\frac{B_r}{P_e^2}\theta\left[\left(\frac{U_{i+1,j}^{k}-U_{i-1,j}^{k}}{2b}\right)^2+\left(\frac{V_{i+1,j}^{k}-V_{i-1,j}^{k}}{2h}\right)^2+\left(\frac{V_{i+1,j}^{k}-V_{i-1,j}^{k}}{2b}+\frac{U_{i,j+1}^{k}-U_{i,j-1}^{k}}{2h}\right)^2\right.$$

$$\left.+\left(\frac{U_{i+1,j}^{k}-U_{i-1,j}^{k}}{2b}\right)^2\right]$$

$$+M_6\left(\frac{\theta_{i+1,j}^{k}-\theta_{i-1,j}^{k}}{2b}+\frac{\theta_{i,j+1}^{k}-\theta_{i,j-1}^{k}}{2h}\right)+N_BR_eP_r\left(\frac{\theta_{i+1,j}^{k}-\theta_{i-1,j}^{k}}{2b}\frac{\phi_{i,j+1}^{k}-\phi_{i,j-1}^{k}}{2b}+\frac{\theta_{i,j+1}^{k}-\theta_{i,j-1}^{k}}{2h}\right.$$

$$\left.\frac{\phi_{i,j+1}^{k}-\phi_{i,j-1}^{k}}{2h}\right)$$

$$+N_TR_eP\left[\left(\frac{\theta_{i+1,j}^{k}-\theta_{i-1,j}^{k}}{2b}\right)^2+\left(\frac{\theta_{i,j+1}^{k}-\theta_{i,j-1}^{k}}{2h}\right)^2\right]$$

C. Discretized concentration equation

International Journal of Recent Development in Engineering and Technology
Website: www.ijrdet.com (ISSN 2347 -6435 (Online)), Volume 14, Issue 12, December 2025)

$$\frac{\phi_{i,j}^{k+1}-\phi_{i,j}^{k}}{n}+U_{i,j,}^{k}\frac{\phi_{i+1,j}^{k}-\phi_{i-1,j}^{k}}{2b}+V_{i,j,}^{k}\frac{\phi_{i,j+1}^{k}-\phi_{i,j-1}^{k}}{2h}$$

$$=\left(\frac{1}{L_e}+M_7\right)\left(\frac{\phi_{i+1,j}^{k}-2\phi_{i,j}^{k}+\phi_{i-1,j}^{k}}{b^2}+\frac{\phi_{i,j+1}^{k}-2\phi_{i,j}^{k}+\phi_{i,j-1}^{k}}{h^2}\right)+$$

$$\frac{1}{L_e}\frac{N_T}{N_B}\left(\frac{\theta_{i+1,j}^{k}-2\theta_{i,j}^{k}+\theta_{i-1,j}^{k}}{b^2}+\frac{\theta_{i,j+1}^{k}-2\theta_{i,j}^{k}+\theta_{i,j-1}^{k}}{h^2}\right)$$

The effect of Re, Gr_T, Gr_C, ϖ and ϕ on the velocity, Re, Br and ϖ on temperature and Le and $\frac{N_T}{N_B}$ on concentration of the fluid are investigated. Given that n=0.001, b=0.025, h=0.025 and applying the boundary conditions U=V=0 and $\theta=\phi=1$.

$$U_{i,j}^{k+1}=U_{i,j}^{k}+1.6M_0P_r(R_e.\omega+1)\left(U_{i+1,j}^{k}-2U_{i,j}^{k}+U_{i-1,j}^{k}\right)$$
$$+1.6M_0P_r\left(U_{i,j+1}^{k}-2U_{i,j}^{k}+U_{i,j-1}^{k}\right)$$
$$+0.4M_1\left(U_{i+1,j+1}^{k}-U_{i+1,j-1}^{k}-U_{i-1,j+1}^{k}+U_{i-1,j-1}^{k}\right)$$
$$+1.6\left(U_{i+1,j}^{k}-2U_{i,j}^{k}+U_{i-1,j}^{k}\right)$$

Taking i = 1,2,3,4,5,6,7…….10 , k= 0 and j =1 ,a system of linear algebraic equations are formed

$$V_{i,j}^{k+1}=V_{i,j}^{k}+1.6M_0P_r(R_e.\omega+1)\left(V_{i,j+1}^{k}-2V_{i,j,}^{k}+V_{i,j-1}^{k}\right)$$
$$+1.6M_0P_r\left(V_{i+1,j}^{k}-2V_{i,j}^{k}+V_{i-1,j}^{k}\right)$$
$$+1.6M_1\left(U_{i,j+1}^{k}-2U_{i,j,k}^{k}+U_{i,j-1}^{k}\right)$$
$$+0.4M_1\left(V_{i+1,j+1}-V_{i+1,j-1}^{k}-V_{i-1,j+1}^{k}+V_{i-1,j-1}^{k}\right)$$
$$.+M_2Gr_TP_r^2+M_2Gr_CP_r^2$$

Taking i = 1,2,3,4,5,6,7…….10 , k= 0 and j =1 ,a system of linear algebraic equations are formed

$$\theta_{i,j}^{k+1}=\theta_{i,j}^{k}+1.6M_4\left(\theta_{i+1,j}^{k}-2\theta_{i,j}^{k}+\theta_{i-1,j}^{k}\right)+$$
$$1.6M_4\left(\theta_{i,j+1}^{k}-2\theta_{i,j}^{k}+\theta_{i,j-1}^{k}\right)+0.02M_5\frac{B_r}{P_e^2}\left(U_{i+1,j}^{k}-U_{i-1,j}^{k}\right)^2$$
$$+0.02M_5\frac{B_r}{P_e^2}\left(V_{i+1,j}^{k}-V_{i-1,j}^{k}\right)^2+$$
$$0.4M_5\frac{B_r}{P_e^2}(V_{i+1,j}^{k}-V_{i-1,j}^{k}+U_{i,j+1}^{k}-U_{i,j-1}^{k})^2$$
$$+0.4M_5\frac{B_r}{P_e^2}(U_{i+1,j}^{k}-U_{i-1,j}^{k})^2+20M_6(\theta_{i+1,j}^{k}-\theta_{i-1,j}^{k})+$$
$$20M_6(\theta_{i,j+1}^{k}-\theta_{i,j-1}^{k})$$
$$+20N_BR_eP_r(\theta_{i+1,j}^{k}-\theta_{i-1,j}^{k})(\phi_{i,j+1}^{k}-\phi_{i,j-1}^{k})+$$
$$20N_BR_eP_r(\theta_{i,j+1}^{k}-\theta_{i,j-1}^{k})(\phi_{i,j+1}^{k}-\phi_{i,j-1}^{k})$$
$$+400N_TR_eP_r(\theta_{i+1,j}^{k}-\theta_{i-1,j}^{k})^2+400N_TR_eP(\theta_{i,j+1}^{k}-\theta_{i,j-1}^{k})^2$$

Taking i = 1,2,3,4,5,6,7…….10 , k = 0 and j =1 ,a system of linear algebraic equations are formed

$$\phi_{i,j}^{k+1}=\phi_{i,j}^{k}+1.6(\frac{1}{L_e}+M_7)\left(\phi_{i+1,j}^{k}-2\phi_{i,j}^{k}+\phi_{i-1,j}^{k}\right)$$
$$+1.6(\frac{1}{L_e}+M_7)\left(\phi_{i,j+1}^{k}-2\phi_{i,j}^{k}+\phi_{i,j-1}^{k}\right)$$
$$+\frac{1.6}{L_e}\frac{N_T}{N_B}\left(\theta_{i+1,j}^{k}-2\theta_{i,j}^{k}+\theta_{i-1,j}^{k}\right)$$
$$+\frac{1.6}{L_e}\frac{N_T}{N_B}\left(\theta_{i,j+1}^{k}-2\theta_{i,j}^{k}+\theta_{i,j-1}^{k}\right)$$

Taking i = 1,2,3,4,5,6,7…….10 , k= 0 and j =1 ,a system of linear algebraic equations are formed.

Solving the above equations in matrix form using MATLAB, we get the velocity, temperature and concentration profiles for varying Re, Gr_T, Gr_C, ϖ , Br , Le , and ϕ

VI. Results and Discussion

This section highlights numerical findings of the effects of varying fluid flow parameters on velocity, temperature and concentration distribution profiles from discretized momentum, energy and concentration equations. The

International Journal of Recent Development in Engineering and Technology
Website: www.ijrdet.com (ISSN 2347 -6435 (Online)), Volume 14, Issue 12, December 2025)

results are given in contours and graphical forms. Further, physical observations are made on the data and discussed by giving scientific explanation.

A. *Velocity profile along the horizontal direction)* for changing Reynolds number

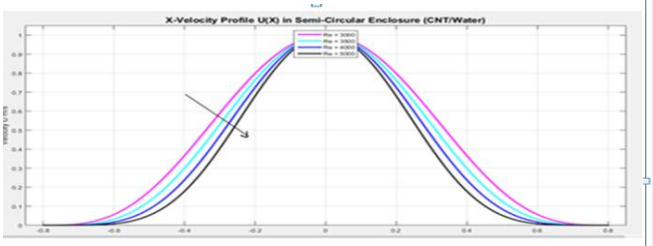

Figure 2: Effect of varying Reynolds number on velocity profile along x direction

Velocity decreases as horizontal distance increases as indicated in Figure 2. The fluid's thermal stratification at the curved wall and the diminishing temperature gradient are the main causes of the velocity decrease. A steeper velocity profile results from increased convective acceleration caused by an increase in Reynolds number. The profile gets narrower and steeper close to the walls as the Reynolds number rises from 3500, 4000, and 5000. This suggests that the fluid experiences steeper velocity gradients close to the boundaries and travels more quickly in the core.

B. *The effects of varying Reynolds number on velocity profile along y-direction*

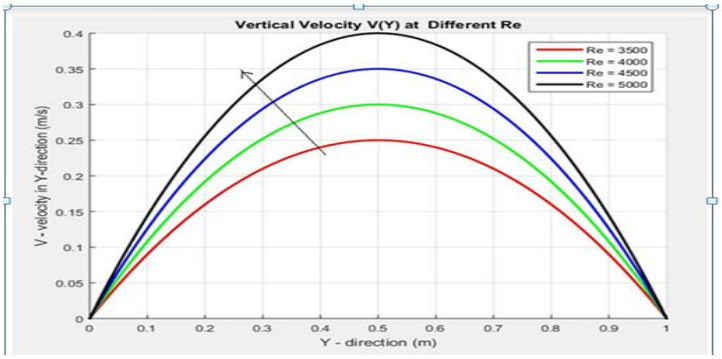

Figure 3: Effects of varying Reynolds number on velocity profile along y-direction

Figure 3: velocity profiles indicate how velocity increases with increasing vertical distance. Since the core is not subject to wall conditions of no slip, the velocity peak is located at y=0.5. Because of the sudden velocity change from wall to core, the velocity gradients near the walls get steeper as the Reynolds number rises.

C. *The effects of Reynolds number on temperature profile along the vertical direction (y-direction)*

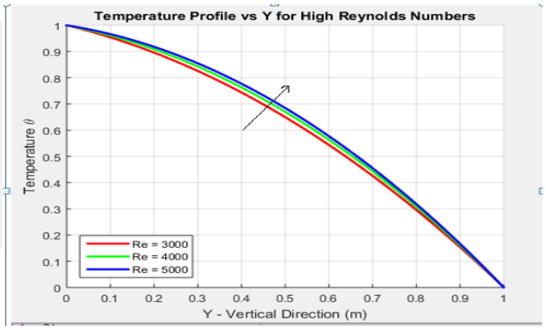

Figure 4: Effects of Reynolds number on temperature profile along the vertical direction (y-direction)

In Figure 4, temperature profile illustrates how temperature decreases with increasing vertical distance. At low Reynolds numbers, the temperature gradient is linear and steep close to the walls. The greater temperature gradient close to the wall is the cause of the steepness. The bulk mixing of the fluid particles resulting from turbulence flow causes the gradient's steepness to decrease in the middle section of the cavity. The temperature profile's gradient is the least steep at the highest Reynolds number (Re = 5000), which indicates strong convection and a nearly uniform temperature in the fluid's bulk.

D. *The effects of thermal Grashof's number on velocity profile along the vertical direction (y-direction)*

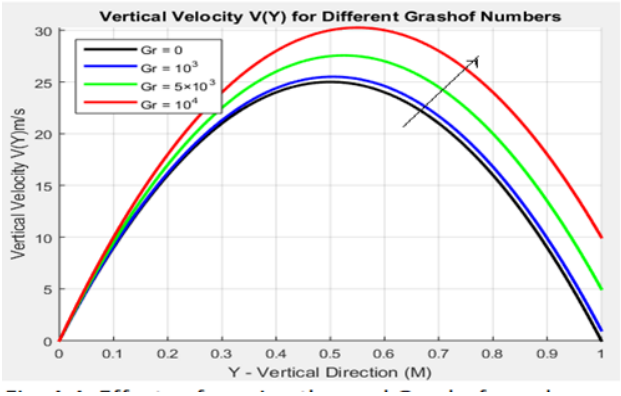

Figure 5: Effects of varying thermal Grashof's number on velocity profile along the vertical direction (y-direction)

International Journal of Recent Development in Engineering and Technology
Website: www.ijrdet.com (ISSN 2347 -6435 (Online)), Volume 14, Issue 12, December 2025)

Figure 5: the velocity profiles show how velocity rises with increasing vertical distance. Since the core is not subject to wall conditions of no slip, the velocity peak is located at y=0.5. Because of the sudden velocity change from wall to core, the velocity gradients get sharper close to the walls as the thermal Grashof number rises. Stronger buoyancy-driven circulation is caused by higher thermal Grashof numbers, which has a major impact on the enclosure's velocity distribution.

E. The effects of mass Grashof's number on velocity profile along the vertical direction (y-direction)

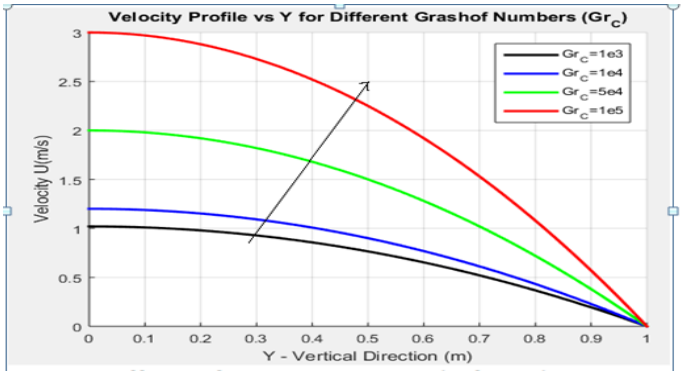

Figure 6: Effects of varying mass Grashof's number on velocity profile along the vertical direction (y-direction)

In Figure 6, the velocity profiles show how velocity decreases with increasing vertical distance. Because buoyancy accelerates the fluid there, velocity starts higher close to the heated wall. The fluid's momentum drops as it enters the enclosure, causing the velocity to drop until it hits zero at symmetry boundaries or walls. The peak velocity gradually increases as GrC rises, indicating the intensification of buoyancy-driven flow brought on by greater solute density gradients.

F. The effects of Brinkman's number on temperature profile along the vertical direction (y-direction)

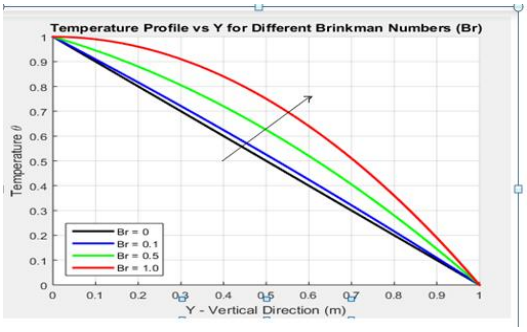

Figure 7: Effects of varying Brinkman's number on temperature profile along the vertical direction (y-direction)

In Figure 7, the temperature profile illustrates how temperature decreases with increasing vertical distance. The middle wall has a less steep profile, and the temperature drops from the horizontal wall to the curved wall. Recirculation and effective fluid particle mixing are attributed to this. More thermal energy is produced internally through fluid friction as the Brinkman number increases, indicating stronger viscous dissipation effects, especially in areas with large velocity gradients.

G. The effects of Lewis number on concentration profile along the vertical direction

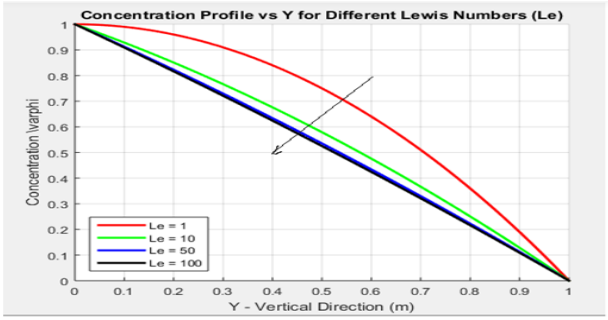

Figure 8: Effects of varying Lewis number on concentration profile along the vertical direction

In Figure 8, the concentration profile illustrates how concentration decreases with increasing vertical distance. From bottom horizontal wall to top curved wall, the concentration decreases, with the middle showing a less steep profile. This results from effective fluid particle mixing and recirculation. In comparison to thermal diffusion, mass diffusion weakens as the Lewis number rises to 10, 50, and 100. As a result, concentration gradients become less steep, and the majority of the nanoparticles remain at the bottom wall.

H. The effects of Heater length ratio parameter on vertical velocity profile.

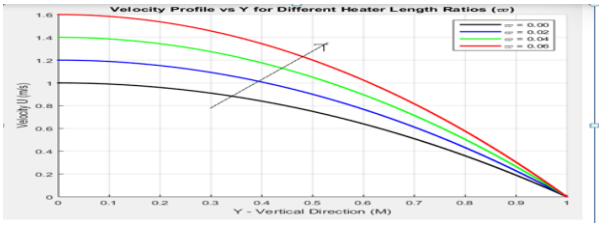

Figure 9: Effects of varying Heater length ratio parameter on vertical velocity profile

International Journal of Recent Development in Engineering and Technology
Website: www.ijrdet.com (ISSN 2347 -6435 (Online)), Volume 14, Issue 12, December 2025)

In Figure 9, the velocity profile illustrates how velocity decreases with increasing vertical distance. Due to the fluid's strong acceleration from localized heating, velocity starts higher close to the heated wall. The fluid's momentum drops as it enters the enclosure, causing the velocity to drop until it hits zero at symmetry boundaries or walls. When heater length ratio rises from 0.00 to 0.06, the maximum velocity is seen to increase. The increased thermal buoyancy effect brought on by increasing the heated surface area is directly responsible for this behavior.

I. The effects of Heater length ratio parameter on temperature contours in the enclosure

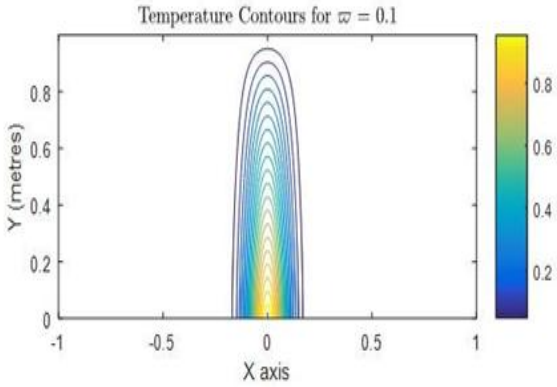

Figure 10: Effects of varying Heater length ratio parameter on temperature contours in the enclosure

Figure 10 shows steep localized gradients caused by a very small heater length ratio. Strong thermal penetration is due to strong conduction close to a horizontal wall. The rest of the enclosure remains colder.

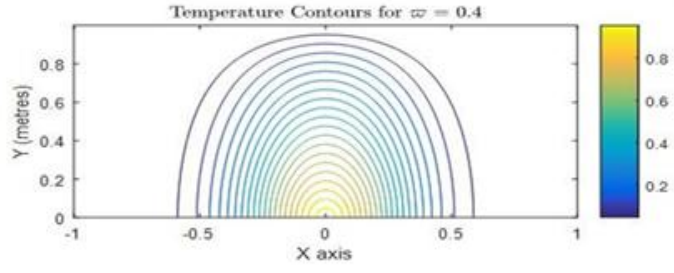

Figure 11: Effects of varying Heater length ratio parameter on temperature contours in the enclosure

In Figure 11, the contours demonstrate the wider heat distribution in the larger heated section. The gradient is less steep than the heater length ratio of 0.1.Heat convection is weakened by weak buoyancy-driven convection due to reduced temperature gradient arising from uniform temperature distribution.

VII. Conclusions and Recommendation

A. Conclusions

The velocity profiles were determined showing strong influence of Thermal Grashof number, mass Grashof number, Reynolds number, heater length ratio and volume fraction. Increasingthe parameters led to thinning boundary layer of velocity profile which has enhanced turbulence mixing hence improving convective heat transfer.

The temperature profiles were determined showing strong influence of Reynolds number, Brinkman's number and heater length ratio. Increasing the Reynolds number leads to thinning thermal boundary layer of temperature profile which has improved convective heat transfer hence enhancing cooling efficiency while increasing Brinkman's number and heater length ratio suppress convective heat transfer due to uniform temperature distribution hence reducing efficiency in cooling.

B. Recommendation

Decreasing Brinkman's number reduced temperature at the core of the enclosure and leads to higher rate of heat transfer. This suggests that fluid of higher thermal conductivity should be employed with greater temperature gradient to maximize thermal efficiency.

The result revealed that Increasing heater length ratio suppress convective heat transfer due to uniform temperature distribution hence reducing efficiency in cooling. A smaller heater electronic chip length ratio should be used in designing electronic cabins.

Study on heating and cooling effects arising from the presence of air in the nanofluid headspace in a semi-circular enclosure should be extended.

VIII. Acknowledgement

The first author thanks Mathematics Department staff at JKUAT Kisii Campus for the support during the period of this study.

References

[1] Alam, M. S., Billah, M. M., Hossain, S. M. C., Keya, S. S., and Haque, M. M. 2022. MHD influence on convective heat transfer in a semi-circular cavity using nonhomogeneous nanofluid model. International Journal of Thermofluids, 16, 100197.

[2] Fang, R. 2025. Numerical analysis of locally adaptive penalty methods for the Navier–Stokes equations. SeMA, https://doi.org/10.1007/s40324-025-00394-8.

[3] Islam, T., Fayz-Al-Asad, M., Khatun, M. A., Parveen, N., Ahmad, H., and Askar, S. 2024. Natural convection heat transport performance of nanofluids under the influence of inclined magnetic field. Results in Physics, *58*, 107365.

[4] Nadeem, S., Siddiqua, A., and Alzabut, J. 2025. Flow of SWCNT and MWCNT based hybrid nanofluids in a semi-circular enclosure with corrugated wall. Advances in Mechanical Engineering, 17(1), 16878132251314272.

[5] Nouraei, S., Anvari, A., Abed, A. M., Akbari, O. A., Montazerifar, F., Baghaei, S., and Fatholahi, M. 2023. Heat transfer and entropy analysis for nanofluid flow in a semi-circular open cavity under mixed convection. Alexandria Engineering Journal, 64, 309-334.

[6] Singh, D. K. 2020. Free convection with MWCNT/water nanofluid having varying aspect ratio of MWCNT nanoparticle in thermally undulated enclosures. International Journal of Mechanical Sciences, *178*, 105626.

[7] Yousefzadeh, S., Eskandari, M., Montazerifar, F., Akbari, O. A., Kahbandeh, F., Khalili, M., and Baghaei, S. 2022. Natural convection of Water/MWCNT nanofluid flow in an enclosure for investigation of the first and second laws of thermodynamics. Alexandria Engineering Journal, 61(12), 11687-11713.